Orbital-Selective Mott Transition Effects and Nontrivial Topology of Iron Chalcogenide

Minjae Kim,[1,2,3,*] Sangkook Choi,[1,4] Walber Hugo Brito,[5,3] and Gabriel Kotliar[3,4]
[1]Korea Institute for Advanced Study, Seoul 02455, South Korea
[2]Department of Chemistry, Pohang University of Science and Technology (POSTECH), Pohang 37673, Korea
[3]Department of Physics and Astronomy, Rutgers University, Piscataway, New Jersey 08854, USA
[4]Condensed Matter Physics and Materials Science Department, Brookhaven National Laboratory, Upton, New York 11973, USA
[5]Departamento de Física, Universidade Federal de Minas Gerais, C. P. 702, 30123-970 Belo Horizonte, MG, Brazil

(Received 11 April 2023; accepted 7 March 2024; published 29 March 2024)

The iron-based superconductor $FeSe_{1-x}Te_x$ has recently gained significant attention as a host of two distinct physical phenomena: (i) Majorana zero modes that can serve as potential topologically protected qubits, and (ii) a realization of the orbital-selective Mott transition. In this Letter, we connect these two phenomena and provide new insights into the interplay between strong electronic correlations and nontrivial topology in $FeSe_{1-x}Te_x$. Using linearized quasiparticle self-consistent *GW* plus dynamical mean-field theory, we show that the topologically protected Dirac surface state has substantial $Fe(d_{xy})$ character. The proximity to the orbital-selective Mott transition plays a dual role: it facilitates the appearance of the topological surface state by bringing the Dirac cone close to the chemical potential but destroys the Z_2 topological superconductivity when the system is too close to the orbital-selective Mott phase. We derive a reduced effective Hamiltonian that describes the topological band. Its parameters capture all the chemical trends found in the first principles calculation. Our findings provide a framework for further study of the interplay between strong electronic correlations and nontrivial topology in other iron-based superconductors.

DOI: 10.1103/PhysRevLett.132.136504

Introduction.—Quantum information science is a surging frontier of physical science. By creating quantum states and utilizing them as quantum bits (qubits) [1], it promises vastly improved performance over what we has been achieved in computing, sensing, communication, and cryptography in the twentieth century [2,3]. Several milestones of quantum technologies, such as universal quantum computers and the notion of quantum supremacy, have been reached successfully. Today's quantum technologies are built on a few tens of qubits. They often suffer from computation-destroying noise [4], spurring the search for bigger and more robust quantum systems. Majorana zero modes are exotic quantum states emerging at the boundary of topological superconductors that provide a topologically protected route to realize qubits [5–7] robust against noise.

Among various topological superconductor candidates, $FeSe_{1-x}Te_x$ (FST) compounds hold an unique position [8–10] as they realize topological superconductivity (TPSC), Majorana states, time-reversal symmetry breaking, a large *s*-wave superconducting gap [11–13], and strong spin-orbit coupling (SOC) in a single material. In the normal phase, parity-even and parity-odd bands are inverted along the $\Gamma - Z$ direction in the first Brillouin zone, and as a result, the SOC opens an energy gap at the band crossing point [8]. This enables nontrivial Z_2 bulk-band topology and "spinless" two-dimensional surface Dirac cone [14–16]. This nontrivial bulk-band topology makes the superconductivity at the surface fascinating. When the chemical potential touches the "spinless" surface state, the bulk *s*-wave superconductivity induces topologically nontrivial superconductivity at the "spinless" surface states [17]. In contrast, the surface states are topologically trivial when the chemical potential is far from the "spinless" surface bands [9]. Following a theoretical prediction [9,17], signatures of Majorana states were found at the core of the vortices and at antiphase structural domain walls of FST [14,18,19].

FST has also been intensively studied as a host of fascinating strong correlation phenomena. It realizes the phenomenon of orbital differentiation (which takes place when some orbitals display significant levels of correlation) and, in its extreme version, the orbital selective Mott phase (OSMP) [20–22]. This phase features a localized $Fe(d_{xy})$ orbital, whereas the rest of the $Fe(d)$ orbitals remain itinerant [20–22]. Up to now, the concepts of Majorana states and OSMP have been addressed separately as independent phenomena. In this Letter, we show that both are intimately connected.

Density-functional theory (DFT) [23,24] is very successful in predicting the topological properties of weakly correlated materials, and it has been used as a standard method for discovery and screening new topological systems. However, it is well-known that DFT fails to describe the strong correlation phenomena, such as the OSMP, which occurs in multiorbital correlated materials.

 © 2024 American Physical Society

Hence, there are important disagreements between DFT bands and experimental observations on FST. For instance, in undoped FST, DFT puts the surface Dirac cone excitation energy ~100 meV above the Fermi level [8,9]. This implies that the surface is topologically trivial in the undoped state, and only becomes nontrivial when the system is sufficiently electron-doped, in stark contrast to the experimental findings [25]. DFT plus dynamical mean-field theory (DMFT) flattens the quasiparticle bands and brings the Dirac surface bands closer to the chemical potential [26].

In this Letter, we demonstrate that the strong orbital-selective correlations and the nontrivial topology of FST are intimately connected. We use linearized quasiparticle self-consistent *GW* (LQS*GW*) [27,28] combined with DMFT [29–37] (LQS*GW* + DMFT) [38,39] to treat static and dynamic correlations. Taking into account both electronic correlation and SOC, we successfully reproduce the bulk-band topology and surface Dirac cone excitation energy of FST. We then derive an effective Hamiltonian to elucidate the character of the band, which disperses along k_z and undergoes band inversion. This turns out to be our main character, the correlated Fe(d_{xy}) orbital, which can undergo an orbital-selective Mott transition (OSMT), rather than the chalcogen p_z orbital as it is usually assumed in the literature [26,40]. We use this Hamiltonian to elucidate the sensitivity of the emerging TPSC of FST to the chemical variations in concentration of Te and to the chalcogen height and conclude that electronic correlations are significant in determining the region of TPSC, which should be not too far but not too close to the OSMT.

Method.—We model the $FeSe_{0.5}Te_{0.5}$ alloy by replacing it by a crystal structure with an averaged chalcogen height, as shown in Figs. 1(a) and 1(b), with parameters adapted from experiments [41,42] (see the Supplemental Material (SM) [43], Sec. I, II.A, III, IV, and V).

The quasiparticle bands of FST were computed using the Hamiltonian

$$H_{\mathrm{LQS}GW+\mathrm{DMFT+SOC}}(k) = H_{\mathrm{LQS}GW+\mathrm{DMFT}}(k) + f_{\text{Fe-}d} Z_{\mathrm{imp}} (\lambda_1 + \Delta\lambda_1)(\mathbf{L}\cdot\mathbf{S}) f^{\dagger}_{\text{Fe-}d} + f_{\text{Se/Te-}p} \lambda_2 (\mathbf{L}\cdot\mathbf{S}) f^{\dagger}_{\text{Se/Te-}p}, \quad (1)$$

where the SOC term was added to the $H_{\mathrm{LQS}GW+\mathrm{DMFT}}(k)$ (see SM [43], Sec. II.B-I). For details of Eq. (1), see Ref. [61]. For the LQS*GW* + DMFT scheme, we used ComDMFT [39]. For more details, see Ref. [63].

Correlated electronic structure and topological superconductivity.—Figures 1(c) and 1(d) display the angle-resolved photoemission (ARPES) quasiparticle dispersions along the $\Gamma - Z$ direction from several experimental groups [8,44,45], and from LQS*GW* + DMFT + SOC quasiparticle dispersions, respectively. Even parity bands of α', α, and β are shown, as well as an odd parity band that is the main character in this Letter. The odd parity band is the most dispersive band along the k_z axis and is responsible for the topological phenomena. We anticipate that this band will be primarily made of a correlated Fe(d_{xy}) orbital close to an OSMT and we anticipate this fact, which will be demonstrated later in this Letter, by using the notation xy^- [see Eq. (2)]. As seen in Fig. 1(d), a SOC-induced gap opens at the band crossing point between α' and xy^- bands. Although there are differences in the energy position of the xy^- band at Z among different experiments, there is consensus that there is a band inversion between the α' and xy^- bands [8,44,45]. Figure 1(c) displays that, in Refs. [44,45], the flat band just beneath the chemical potential undergoes a switch of band character (parity) from α' (+) to xy^- (−) in the $\Gamma - Z$ direction, which is similar to the recent ARPES study on this compound in Ref. [65]. In contrast, in Ref. [8], the energy position of the xy^- band at Z is at least below −0.2 eV.

Figure 1(d) presents the electronic structure obtained within the LQS*GW* + DMFT + SOC method along $\Gamma - Z$. The chemical potential lies within the SOC-induced gap, which is in agreement with ARPES experiments [8,44,45]. The even-parity α' band lies below the chemical potential at Γ and above it at Z, while the odd-parity xy^- band lies

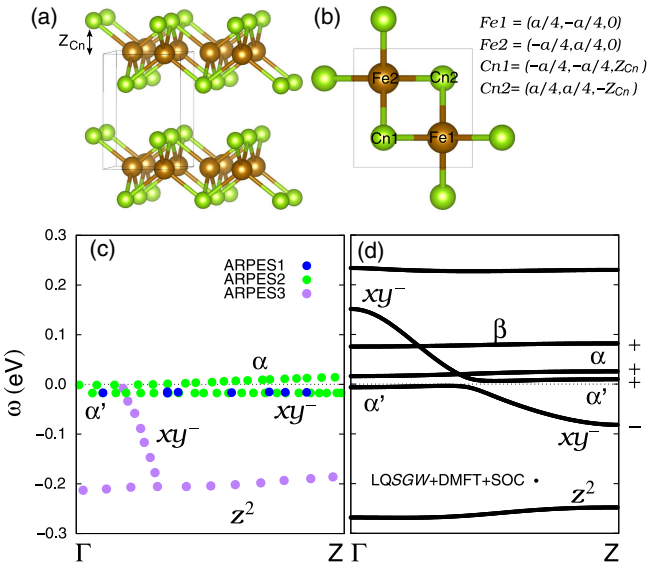

FIG. 1. Structural inversion symmetry, and the band inversion in experiments [8,44,45] and the present theory. (a),(b) The present structural model for FST and the atomic coordinate in the unit cell. The Cn indicates a chalcogen atom, and the inversion center is [0,0,0]. (c) Experimental quasiparticle dispersions in the $\Gamma - Z$ k point line, adapted from P. D. Johnson *et al.* (ARPES1 from Ref. [44]), H. Lohani *et al.* (ARPES2 from Ref. [45]), and Z. Wang *et al.* (ARPES3 from Ref. [8]). (d) Theoretical quasiparticle dispersions in the $\Gamma - Z$ k point line in the present LQSGW + DMFT + SOC framework. Parity eigenvalues for each band are denoted in (d), as α' (+), α (+), β (+), and xy^- (−). The band has the z^2 orbital character is also denoted in (c) and (d).

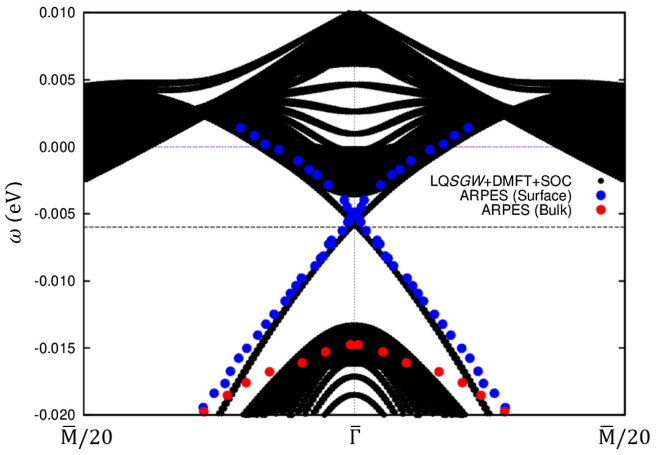

FIG. 2. Theoretical (001) surface state electronic structure in the LQSGW + DMFT + SOC near $\bar{\Gamma}$, compared with the experimental surface electronic structure in the ARPES of Ref. [14]. The black horizontal dashed line is the original chemical potential in the present theory. The purple horizontal dashed line is the chemical potential for the electron doping of 0.035 (electrons/formula unit), +6 meV in the present theory.

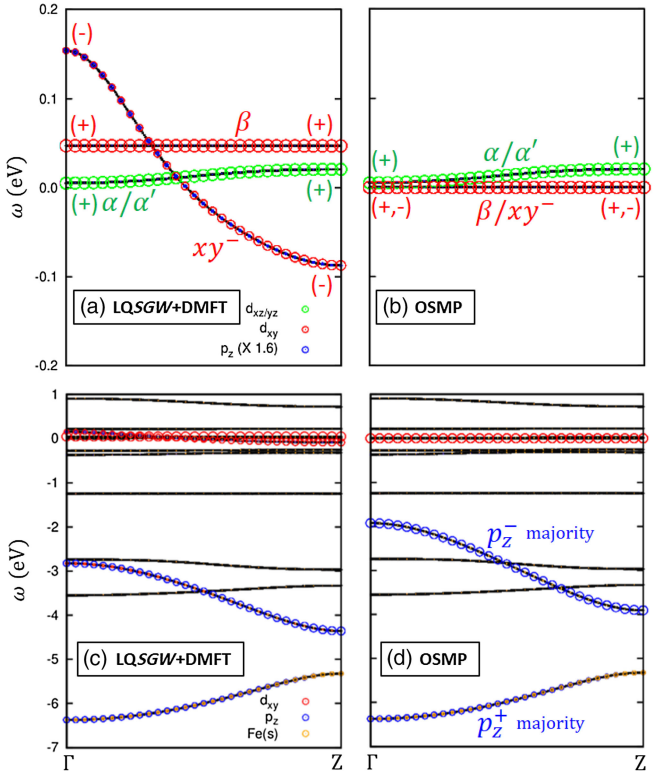

FIG. 3. OSMT effects on the electronic structure of FST. (a) Band structure of FST in the LQSGW + DMFT framework. (b) Band structure of FST in the OSMP by forcing Z_{xy} to zero from the LQSGW + DMFT result. (c) and (d) are the same as (a) and (b) in a wide energy window, respectively. The size of green, red, blue, and orange circles present Fe($d_{xz/yz}$), Fe(d_{xy}), Se(p_z), and Fe(s) orbital contributions, respectively. For (a) and (b), the size of blue circles for the Se(p_z) orbital is multiplied by the factor of 1.6. The parity for α, α', β, and xy^- bands are denoted in (a) and (b). The characterization of p_z^- majority and p_z^+ majority bands are denoted for (c) and (d) [see Eq. (2)].

above the chemical potential at Γ and below it at Z. This band inversion, in the presence of time-reversal and inversion symmetries, leads to a nontrivial Z_2 invariant at the bulk, resulting in the emergence of a surface state Dirac cone at Γ in the (001) surface. Our calculations are in good agreement with ARPES experiments [8,44,45], indicating that they properly describe the topological properties of the material. Interestingly, the energy position of the xy^- band at Z obtained by the present theory lies between the experiments of Refs. [44,45] and Ref. [8]. This has been attributed to the sensitivity of the xy^- band dispersion to the orbital-selective correlation of the Fe(d_{xy}) orbital, which is affected by the Se/Te ratio. Additionally, the energy position of the Fe(d_{z^2}) driven bands is in agreement with the experiment of Ref. [8]. This confirms the effectiveness of the LQSGW + DMFT + SOC framework in treating electronic correlations.

Figure 2 displays the surface electronic structure near $\bar{\Gamma}$ obtained from a slab calculation using the bulk LQSGW + DMFT + SOC parameters (see SM [43], Sec. II.J). The surface state Dirac cone of this theory is in excellent agreement with the ARPES data reported in Ref. [14] after a small chemical potential shift of +6 meV (0.035 electrons/formula unit). Hence, the present theoretical tools can be used for the quantitative description of the TPSC of FST. This agreement requires the following important ingredients: (i) the static self-energy driven lowering of the Fe($d_{xz/yz}$) orbital energy level, (ii) the dynamical correlation driven renormalization of bands, and (iii) the renormalized SOC from the consideration of the orbitally off-diagonal self-energy.

Orbital-selective Mott transition and nontrivial Z_2 topology.—We now demonstrate the assertion that the most dispersive band along k_z, has a dominant Fe(d_{xy}) orbital contribution hybridizing with the Se(p_z) orbital justifying our label xy^-. The band inversion in this band drives the Z_2 topology. Its sensitivity to the orbital selective correlation derives from its dominant Fe(d_{xy}) orbital character depicted in Fig. 3. This is not widely recognized in the literature and this band is often labeled as a p_z band in the literature [26,40].

Analysis of Fig. 3 reveals that the OSMT in FST removes the nontrivial Z_2 topology of the bulk from the xy^- band, as the β (even parity) and xy^- (odd parity) bands merge to identical flat bands at the chemical potential, with the loss of spectral weights due to the incoherent nature of the Fe(d_{xy}) orbital in the OSMP (for details of the chalcogen height or the Te ratio enhancement driven promotion of the orbital selective electronic correlation approaching the OSMP, see SM [43], Sec. IV and V). This explains the

disappearance of the Dirac band from the enhancement of the Te ratio in the experiment [25] (details of the Z_2 topology are in the SM [43], Sec. VI).

We now construct an effective Hamiltonian in Eq. (2) to analyze the relation between the nontrivial Z_2 topology and the substantial correlation strength in the Fe(d_{xy}) orbital. The Hamiltonian, $H_{mn}(0,0,k_z)$, is initially constructed in the basis of two Fe(d_{xy}) orbitals ($|xy1\rangle$ and $|xy2\rangle$) and two Se(p_z) orbitals ($|p_z1\rangle$ and $|p_z2\rangle$) in the unit cell, and was transformed to the crystal momentum space with $k_{x,y}$ set to 0 for the $\Gamma - Z$ momentum path. We transform the Hamiltonian $H_{mn}(0,0,k_z)$ to the $H_{\tilde{m}\tilde{n}}(0,0,k_z)$ in Eq. (2) using the basis transformation as $|xy^-\rangle = (1/\sqrt{2})(|xy1\rangle - |xy2\rangle)$, $|xy^+\rangle = (1/\sqrt{2})(|xy1\rangle + |xy2\rangle)$, $|p_z^-\rangle = (1/\sqrt{2})(|p_z1\rangle + |p_z2\rangle)$, and $|p_z^+\rangle = (1/\sqrt{2})(|p_z1\rangle - |p_z2\rangle)$. The Hamiltonian $H_{\tilde{m}\tilde{n}}(0,0,k_z)$ in Eq. (2) is in the order of $|xy^-\rangle$, $|xy^+\rangle$, $|p_z^-\rangle$, and $|p_z^+\rangle$ basis. In this basis, $+$ and $-$ signs denote even and odd parities, respectively [66]. The tight-binding parameters in Eq. (2) are effective variables that encompass contributions from longer range hoppings and other dispersive orbitals [e.g., Fe(s) in Fig. 3]. The on-site energy level of an orbital m is $\tilde{\epsilon}_m$, and the nearest neighboring hopping within the orbital is $\tilde{t}_m$. The out-of-plane hopping of Se(p_z) is $\tilde{t}_2$, and the nearest hopping between Fe(d_{xy}) and Se(p_z) is $\tilde{t}_1$. All hopping elements are real and positive, thus accounting for the parity of four orbitals (see SM [43], Sec. VII):

$$H_{\tilde{m}\tilde{n}}(0,0,k_z) = \begin{bmatrix} \tilde{\epsilon}_{xy} - 4\tilde{t}_{xy} & 0 & 4\tilde{t}_1 & 0 \\ 0 & \tilde{\epsilon}_{xy} + 4\tilde{t}_{xy} & 0 & 0 \\ 4\tilde{t}_1 & 0 & \tilde{\epsilon}_{p_z} + 4\tilde{t}_{p_z} + 4\tilde{t}_2 \cos k_z & -4i\tilde{t}_2 \sin k_z \\ 0 & 0 & +4i\tilde{t}_2 \sin k_z & \tilde{\epsilon}_{p_z} - 4\tilde{t}_{p_z} - 4\tilde{t}_2 \cos k_z \end{bmatrix}. \quad (2)$$

Equation (2) reveals that the $|xy^+\rangle$ basis does not hybridize with any other vector in the basis at $\Gamma - Z$, and can be regarded as a nonbonding state of Fe(d_{xy}). The band associated with this orbital character is the β band, which is consistent with Eq. (2) as it has an even parity with very weak dispersion in $\Gamma - Z$, as shown in Fig. 1. In contrast, the $|xy^-\rangle$ orbital hybridizes with the $|p_z^-\rangle$ orbital from the $4\tilde{t}_1$ term in Eq. (2), which is allowed by the inversion symmetry of the system [8]. The band resulting from this hybridization, the xy^- band in Fig. 1, has odd parity. It is important to note that the xy^- band is primarily composed of the Fe(d_{xy}) orbital due to the substantially higher energy level of the $|xy^-\rangle$ orbital than that of the $|p_z^-\rangle$ orbital in Eq. (2), as shown in Figs. 3(a) and 3(c). The xy^- band acquires a band dispersion in k_z from the $4\tilde{t}_1$ term [67].

All the first principles studies were carried out at a composition with equal amounts of Se and Te. We now construct a simple model to understand analytically the effects of increasing Te or increasing chalcogen height, which results in increasing correlation strength that affects the electronic structure, summarized by Eq. (2). We use the mass renormalization parameters of the Fe(d) orbital, Z_m of the d orbital m, which decrease as the correlation strength increases, renormalizing the hoppings from their bare value to $\sqrt{Z_m}t_{mn}\sqrt{Z_n}$. Z_{xy} approaches zero when the correlation is enhanced with a larger Te ratio [20,21]. We conclude that the reduction of the $\tilde{t}_1$ term from the OSMT in FST leads to a down shifted energy level of the xy^- band, as well as a decrease in the k_z dependent dispersion of the xy^- band:

$$\tilde{t}_1 \to \sqrt{Z_{xy}}\tilde{t}_1, \quad \tilde{t}_{xy} \to Z_{xy}\tilde{t}_{xy}. \quad (3)$$

Equation (3) demonstrates the renormalization of hopping elements, $\tilde{t}_1$ and $\tilde{t}_{xy}$, due to the dynamical correlation of the Fe(d_{xy}) orbital. Through Eq. (2) and Eq. (3), it is evident that in the vicinity of the OSMP, the two Fe(d_{xy}) dominant bands, β and xy^-, coalesce into a single flat band due to the lack of hybridization with the $|p_z^-\rangle$ orbital. This implies that close to the OSMP, the Z_2 topology is trivial, with a removal of band inversion between the α' and xy^- bands, which is consistent with the band structure in Figs. 3(b) and 3(d). The effective Hamiltonian in Eq. (2) successfully captures the electronic structure in Fig. 3 (see SM [43], Sec. VII).

In Fig. 4, we present the Z_{Se} dependent top and bottom energy positions of the α/α' band and the xy^- band in $\Gamma - Z$ from the local density approximation (LDA), the LQSGW, and the LQSGW + DMFT frameworks. The range of the Z_{Se} for the band inversion gives rise to the nontrivial Z_2 topology is determined to be [1.38,1.61] Å for the LDA, [1.41,1.52] Å for the LQSGW, and [1.42,1.51] Å for the LQSGW + DMFT, respectively, as shown in Figs. 4(a)–4(c) from the band inversion condition in Fig. 4(d) [68]. The electronic correlation renormalizes the bandwidth of the xy^- band, reducing the range of Z_{Se} for the nontrivial Z_2 topology. It is also found that the electronic correlation shifts down the α/α' band with the reduced bandwidth of the band. The electronic correlation effects on the xy^- band explains the removal of the TPSC of FST upon enhancing Te or Se ratio, which changes the chalcogen heights [25] (see SM [43], Sec. IV and V). Furthermore, in the DFT framework, the substitution of Te for Se brings a minor enhancement of the $\tilde{t}_1$ term while

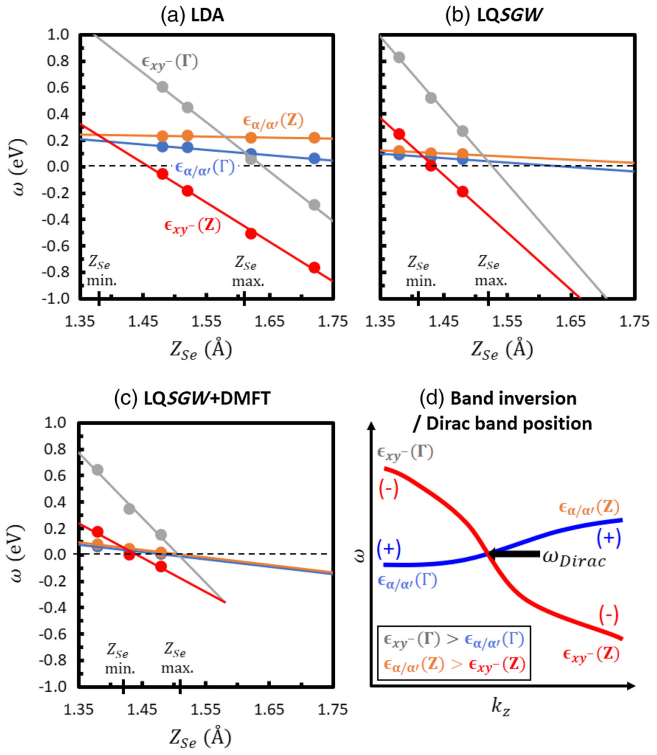

FIG. 4. The Z_{Se} dependent phase diagram of the band inversion condition for the nontrivial Z_2 bulk topology and the energy position of the Dirac surface band. (a) The Z_{Se} dependent variation of (i) the α/α' bands top and bottom energy positions [$\epsilon_{\alpha/\alpha'}(Z)$ and $\epsilon_{\alpha/\alpha'}(\Gamma)$], and (ii) the xy^- band top and bottom energy positions [$\epsilon_{xy^-}(\Gamma)$ and $\epsilon_{xy^-}(Z)$]. The α/α' bands degenerate along the $\Gamma - Z$ momentum path in computations without SOC. Linear lines are for the interpolating from the given data (dots) in the LDA. [$Z_{Se,min}$, $Z_{Se,max}$] indicate the range of the Z_{Se} for the band inversion. (b) Same as (a) in the LQSGW. (c) Same as (a) in the LQSGW + DMFT. (d) A schematic diagram for the band inversion condition and the energy position (ω_{Dirac}) for the Dirac surface band.

substantially enhancing the $\tilde{t}_2$ term, leading to the OSMP with vanishing $\tilde{t}_1$ contribution (see SM [43], Sec. VIII [69]). These results demonstrate the essential roles of the electronic correlation for the observation of the TPSC in FST.

Conclusion.—Recognizing the correlated nature of the topologically nontrivial band [Fe(d_{xy}) xy^-, which drives the OSMT] provides new insights into many puzzling observations of FST. As the surface of a layered compound is more correlated than the bulk layers due to reduced screening, we expect the surface OSMT to occur at a larger Se concentration than in the bulk. In the OSMP, Fe(d_{xy}) surface local moments are coupled to the itinerant states of Fe($d_{xz/yz}$) via double exchange, leading to possible time-reversal symmetry breaking states, accounting for the recent experimental observations [10,16].

Quantitatively, the successful application of the LQSGW + DMFT + SOC method enabled the theoretical estimations of the parameters of TPSC of FST and their dependence on the structure and the chemistry of the compound. We provided an explanation for the region of TPSC found in the phase diagram of Refs. [10,25], which we demonstrated requires an intermediate concentration of Te so as to be close but not too close to the OSMP. This suggests that theoretically guided correlated topological material design is feasible. More detailed modeling of the interplay of surface and bulk phenomena will required extensions of the quasiparticle GW + DMFT techniques to strongly inhomogeneous states [70].

Finally, the strong sensitivity of the topological band to the chalcogen height suggests experiments using stress [71] to control the region of the phase diagram realizing TPSC with its resulting Majorana zero modes to test our understanding of this material further.

We are grateful to Youngkuk Kim for discussions with S. C. and to Tamaghna Hazra for discussions with G. K. G. K. and S. C. both acknowledge comments and discussions with P. Johnson and A. Tsvelik. This work was supported by the U.S. Department of Energy, Office of Science, Basic Energy Sciences as a part of the Computational Materials Science Program. The *ab initio* LQSGW + DMFT calculation used resources of the National Energy Research Scientific Computing Center (NERSC), a U.S. Department of Energy Office of Science User Facility operated under Contract No. DE-AC02-05CH11231. M. K. was supported by a KIAS Individual Grant No. (CG083501) at Korea Institute for Advanced Study. S. C. was supported by a KIAS Individual Grant (CG090601) at Korea Institute for Advanced Study. Part of the DFT and the LQSGW + DMFT calculation is supported by the Center for Advanced Computation at Korea Institute for Advanced Study.

*Corresponding author: garix.minjae.kim@gmail.com

[1] D. P. DiVincenzo, The physical implementation of quantum computation, Fortschr. Phys. **48**, 771 (2000).
[2] J. P. Dowling and G. J. Milburn, Quantum technology: The second quantum revolution, Phil. Trans. R. Soc. A **361**, 1655 (2003).
[3] M. Atzori and R. Sessoli, The second quantum revolution: Role and challenges of molecular chemistry, J. Am. Chem. Soc. **141**, 11339 (2019).
[4] J. Preskill, Quantum computing in the NISQ era and beyond, Quantum **2**, 79 (2018).
[5] A. Y. Kitaev, Unpaired Majorana fermions in quantum wires, Phys. Usp. **44**, 131 (2001).
[6] A. Y. Kitaev, Fault-tolerant quantum computation by anyons, Ann. Phys. (Amsterdam) **303**, 2 (2003).
[7] N. Read and D. Green, Paired states of fermions in two dimensions with breaking of parity and time-reversal symmetries and the fractional quantum Hall effect, Phys. Rev. B **61**, 10267 (2000).
[8] Z. Wang, P. Zhang, G. Xu, L. K. Zeng, H. Miao, X. Xu, T. Qian, H. Weng, P. Richard, A. V. Fedorov, H. Ding, X. Dai,

and Z. Fang, Topological nature of the $FeSe_{0.5}Te_{0.5}$ superconductor, Phys. Rev. B **92**, 115119 (2015).
[9] G. Xu, B. Lian, P. Tang, X.-L. Qi, and S.-C. Zhang, Topological superconductivity on the surface of Fe-based superconductors, Phys. Rev. Lett. **117**, 047001 (2016).
[10] C. Farhang, N. Zaki, J. Wang, G. Gu, P. D. Johnson, and J. Xia, Revealing the origin of time-reversal symmetry breaking in fe-chalcogenide superconductor $FeTe_{1-x}Se_x$, Phys. Rev. Lett. **130**, 046702 (2023).
[11] K.-W. Yeh, T.-W. Huang, Y.-l. Huang, T.-K. Chen, F.-C. Hsu, P. M. Wu, Y.-C. Lee, Y.-Y. Chu, C.-L. Chen, J.-Y. Luo, D.-C. Yan, and M.-K. Wu, Tellurium substitution effect on superconductivity of the alpha-phase iron selenide, Europhys. Lett. **84**, 37002 (2008).
[12] M. H. Fang, H. M. Pham, B. Qian, T. J. Liu, E. K. Vehstedt, Y. Liu, L. Spinu, and Z. Q. Mao, Superconductivity close to magnetic instability in $Fe(Se_{1-x}Te_x)_{0.82}$, Phys. Rev. B **78**, 224503 (2008).
[13] B. C. Sales, A. S. Sefat, M. A. McGuire, R. Y. Jin, D. Mandrus, and Y. Mozharivskyj, Bulk superconductivity at 14 K in single crystals of $Fe_{1+y}Te_xSe_{1-x}$, Phys. Rev. B **79**, 094521 (2009).
[14] P. Zhang, K. Yaji, T. Hashimoto, Y. Ota, T. Kondo, K. Okazaki, Z. Wang, J. Wen, G. Gu, H. Ding *et al.*, Observation of topological superconductivity on the surface of an iron-based superconductor, Science **360**, 182 (2018).
[15] J. D. Rameau, N. Zaki, G. D. Gu, P. D. Johnson, and M. Weinert, Interplay of paramagnetism and topology in the Fe-chalcogenide high-T_c superconductors, Phys. Rev. B **99**, 205117 (2019).
[16] N. Zaki, G. Gu, A. Tsvelik, C. Wu, and P. D. Johnson, Time-reversal symmetry breaking in the Fe-chalcogenide superconductors, Proc. Natl. Acad. Sci. U.S.A. **118**, e2007241118 (2021).
[17] L. Fu and C. L. Kane, Superconducting proximity effect and Majorana fermions at the surface of a topological insulator, Phys. Rev. Lett. **100**, 096407 (2008).
[18] D. Wang, L. Kong, P. Fan, H. Chen, S. Zhu, W. Liu, L. Cao, Y. Sun, S. Du, J. Schneeloch *et al.*, Evidence for Majorana bound states in an iron-based superconductor, Science **362**, 333 (2018).
[19] Z. Wang, J. O. Rodriguez, L. Jiao, S. Howard, M. Graham, G. Gu, T. L. Hughes, D. K. Morr, and V. Madhavan, Evidence for dispersing 1d Majorana channels in an iron-based superconductor, Science **367**, 104 (2020).
[20] M. Yi, Z. Liu, Y. Zhang, R. Yu, J.-X. Zhu, J. Lee, R. Moore, F. Schmitt, W. Li, S. Riggs *et al.*, Observation of universal strong orbital-dependent correlation effects in iron chalcogenides, Nat. Commun. **6**, 1 (2015).
[21] J. Huang, R. Yu, Z. Xu, J.-X. Zhu, J. S. Oh, Q. Jiang, M. Wang, H. Wu, T. Chen, J. D. Denlinger *et al.*, Correlation-driven electronic reconstruction in $FeTe_{1-x}Se_x$, Commun. Phys. **5**, 1 (2022).
[22] H. Miao, W. H. Brito, Z. P. Yin, R. D. Zhong, G. D. Gu, P. D. Johnson, M. P. M. Dean, S. Choi, G. Kotliar, W. Ku, X. C. Wang, C. Q. Jin, S. F. Wu, T. Qian, and H. Ding, Universal $2\Delta_{\max}/k_BT_c$ scaling decoupled from the electronic coherence in iron-based superconductors, Phys. Rev. B **98**, 020502(R) (2018).
[23] P. Hohenberg and W. Kohn, Inhomogeneous electron gas, Phys. Rev. **136**, B864 (1964).
[24] W. Kohn and L. J. Sham, Self-consistent equations including exchange and correlation effects, Phys. Rev. **140**, A1133 (1965).
[25] Y. Li, N. Zaki, V. O. Garlea, A. T. Savici, D. Fobes, Z. Xu, F. Camino, C. Petrovic, G. Gu, P. D. Johnson *et al.*, Electronic properties of the bulk and surface states of $Fe_{1+y}Te_{1-x}Se_x$, Nat. Mater. **20**, 1221 (2021).
[26] X. Ma, G. Wang, R. Liu, T. Yu, Y. Peng, P. Zheng, and Z. Yin, Correlation-corrected band topology and topological surface states in iron-based superconductors, Phys. Rev. B **106**, 115114 (2022).
[27] A. Kutepov, K. Haule, S. Y. Savrasov, and G. Kotliar, Electronic structure of Pu and Am metals by self-consistent relativistic GW method, Phys. Rev. B **85**, 155129 (2012).
[28] A. Kutepov, V. Oudovenko, and G. Kotliar, Linearized self-consistent quasiparticle GW method: Application to semiconductors and simple metals, Comput. Phys. Commun. **219**, 407 (2017).
[29] A. Georges, G. Kotliar, W. Krauth, and M. J. Rozenberg, Dynamical mean-field theory of strongly correlated fermion systems and the limit of infinite dimensions, Rev. Mod. Phys. **68**, 13 (1996).
[30] W. Metzner and D. Vollhardt, Correlated lattice fermions in $d = \infty$ dimensions, Phys. Rev. Lett. **62**, 324 (1989).
[31] E. Müller-Hartmann, Correlated fermions on a lattice in high dimensions, Z. Phys. B Condens. Matter **74**, 507 (1989).
[32] U. Brandt and C. Mielsch, Thermodynamics and correlation functions of the Falicov-Kimball model in large dimensions, Z. Phys. B Condens. Matter **75**, 365 (1989).
[33] V. Janiš, A new construction of thermodynamic mean-field theories of itinerant fermions: Application to the Falicov-Kimball model, Z. Phys. B Condens. Matter **83**, 227 (1991).
[34] A. Georges and G. Kotliar, Hubbard model in infinite dimensions, Phys. Rev. B **45**, 6479 (1992).
[35] M. Jarrell, Hubbard model in infinite dimensions: A quantum Monte Carlo study, Phys. Rev. Lett. **69**, 168 (1992).
[36] M. J. Rozenberg, X. Y. Zhang, and G. Kotliar, Mott-Hubbard transition in infinite dimensions, Phys. Rev. Lett. **69**, 1236 (1992).
[37] A. Georges and W. Krauth, Numerical solution of the $d = \infty$ Hubbard model: Evidence for a Mott transition, Phys. Rev. Lett. **69**, 1240 (1992).
[38] S. Choi, A. Kutepov, K. Haule, M. van Schilfgaarde, and G. Kotliar, First-principles treatment of Mott insulators: linearized QSGW+DMFT approach, npj Quantum Mater. **1**, 16001 (2016).
[39] S. Choi, P. Semon, B. Kang, A. Kutepov, and G. Kotliar, ComDMFT: a massively parallel computer package for the electronic structure of correlated-electron systems, Comput. Phys. Commun. **244**, 277 (2019).
[40] R. M. Fernandes, A. I. Coldea, H. Ding, I. R. Fisher, P. Hirschfeld, and G. Kotliar, Iron pnictides and chalcogenides: A new paradigm for superconductivity, Nature (London) **601**, 35 (2022).
[41] M. Tegel, C. Löhnert, and D. Johrendt, The crystal structure of $FeSe_{0.44}Te_{0.56}$, Solid State Commun. **150**, 383 (2010).

[42] S. Li, C. de la Cruz, Q. Huang, Y. Chen, J. W. Lynn, J. Hu, Y.-L. Huang, F.-C. Hsu, K.-W. Yeh, M.-K. Wu, and P. Dai, First-order magnetic and structural phase transitions in $Fe_{1+y}Se_xTe_{1-x}$, Phys. Rev. B **79**, 054503 (2009).

[43] See Supplemental Material at http://link.aps.org/supplemental/10.1103/PhysRevLett.132.136504 for (i) a comparison of ARPES and the present theory, (ii) computational details, (iii) the definition of the projector $f_{\text{Fe}-d\ or\ \text{Se/Te}-p}$, (iv) the extraction of the spin-orbit coupling (SOC) constants, (v) the computation of surface electronic structures, (vi) the SOC enhancement and chalcogen heights, (vii) a comparison of the local density approximation (LDA) electronic structures and essential low energy parameters with the FeTe and FeSe chemical formula in the lattice constant of $FeSe_{0.5}Te_{0.5}$ with the consideration of the variation in the chalcogen heights, (viii) tight-binding parameters and electronic structures from the linearized quasiparticle self-consistent *GW* (LQS*GW*) and the LQS*GW* plus dynamical mean-field theory (LQS*GW* + DMFT), (ix) a detailed discussion on the Z_2 topology and OSMP, (x) the effective tight-binding parameters in the Hamiltonian of Eq. (2) and its comparison to the LQS*GW* + DMFT result in Fig. 3, (xi) the chalcogen height or the Te ratio enhancement driven promotion of the orbital-selective electronic correlation approaching the orbital-selective Mott phase, and (xii) the correspondence between the Te concentration in the FST alloy and the chalcogen height in the present coherent lattice approximation, which includes Refs. [8,9,14,21,22,28,41,42,44–60].

[44] P. D. Johnson, H.-B. Yang, J. D. Rameau, G. D. Gu, Z.-H. Pan, T. Valla, M. Weinert, and A. V. Fedorov, Spin-orbit interactions and the nematicity observed in the Fe-based superconductors, Phys. Rev. Lett. **114**, 167001 (2015).

[45] H. Lohani, T. Hazra, A. Ribak, Y. Nitzav, H. Fu, B. Yan, M. Randeria, and A. Kanigel, Band inversion and topology of the bulk electronic structure in $FeSe_{0.45}Te_{55}$, Phys. Rev. B **101**, 245146 (2020).

[46] M. Kim, J. Mravlje, M. Ferrero, O. Parcollet, and A. Georges, Spin-orbit coupling and electronic correlations in Sr_2RuO_4, Phys. Rev. Lett. **120**, 126401 (2018).

[47] A. Tamai, M. Zingl, E. Rozbicki, E. Cappelli, S. Ricco, A. de la Torre, S. Mc Keown Walker, F. Y. Bruno, P. D. C. King, W. Meevasana *et al.*, High-resolution photoemission on Sr_2RuO_4 reveals correlation-enhanced effective spin-orbit coupling and dominantly local self-energies, Phys. Rev. X **9**, 021048 (2019).

[48] N.-O. Linden, M. Zingl, C. Hubig, O. Parcollet, and U. Schollwöck, Imaginary-time matrix product state impurity solver in a real material calculation: Spin-orbit coupling in Sr_2RuO_4, Phys. Rev. B **101**, 041101(R) (2020).

[49] P. Blaha, K. Schwarz, G. K. Madsen, D. Kvasnicka, and J. Luitz, WIEN2K, An APW + lo program for calculating the properties of solids, J. Chem. Phys. **152**, 074101 (2020).

[50] A. A. Mostofi, J. R. Yates, Y.-S. Lee, I. Souza, D. Vanderbilt, and N. Marzari, Wannier90: A tool for obtaining maximally-localised Wannier functions, Comput. Phys. Commun. **178**, 685 (2008).

[51] J. M. Tomczak, P. Liu, A. Toschi, G. Kresse, and K. Held, Merging GW with DMFT and non-local correlations beyond, Eur. Phys. J. Special Topics **226**, 2565 (2017).

[52] A. J. Kim, P. Werner, and R. Valentí, Alleviating the sign problem in quantum Monte Carlo simulations of spin-orbit-coupled multiorbital Hubbard models, Phys. Rev. B **101**, 045108 (2020).

[53] D. Phelan, J. N. Millican, E. L. Thomas, J. B. Leao, Y. Qiu, and R. Paul, Neutron scattering measurements of the phonon density of states of $FeSe_{1-x}$ superconductors, Phys. Rev. B **79**, 014519 (2009).

[54] Y. Mizuguchi, F. Tomioka, S. Tsuda, T. Yamaguchi, and Y. Takano, FeTe as a candidate material for new iron-based superconductor, Physica (Amsterdam) **469C**, 1027 (2009).

[55] K. Haule, C.-H. Yee, and K. Kim, Dynamical mean-field theory within the full-potential methods: Electronic structure of $CeIrIn_5$, $CeCoIn_5$, and $CeRhIn_5$, Phys. Rev. B **81**, 195107 (2010).

[56] K. Haule, Quantum Monte Carlo impurity solver for cluster dynamical mean-field theory and electronic structure calculations with adjustable cluster base, Phys. Rev. B **75**, 155113 (2007).

[57] Z. P. Yin, K. Haule, and G. Kotliar, Fractional power-law behavior and its origin in iron-chalcogenide and ruthenate superconductors: Insights from first-principles calculations, Phys. Rev. B **86**, 195141 (2012).

[58] F. B. Kugler and G. Kotliar, Is the orbital-selective Mott phase stable against interorbital hopping?, Phys. Rev. Lett. **129**, 096403 (2022).

[59] R. Yu and Q. Si, Orbital-selective Mott phase in multiorbital models for iron pnictides and chalcogenides, Phys. Rev. B **96**, 125110 (2017).

[60] V. Cvetkovic and O. Vafek, Space group symmetry, spin-orbit coupling, and the low-energy effective Hamiltonian for iron-based superconductors, Phys. Rev. B **88**, 134510 (2013).

[61] $f_{\text{Fe-}d/\text{Se-}p/\text{Te-}p}$ is the projection operator to Fe-d, Se-p, and Te-p orbitals. $Z_{\text{imp}}(\lambda_1 + \Delta\lambda_1)$ is the quasiparticle SOC of Fe(d) orbital renormalized from electronic correlations [46–48,62]. λ_2 is the average of the SOC of Se/Te(p) states (see SM [43], Sec. II.H-I).

[62] M. Kim, H. Miao, S. Choi, M. Zingl, A. Georges, and G. Kotliar, Spatial locality of electronic correlations in LiFeAs, Phys. Rev. B **103**, 155107 (2021).

[63] ComDMFT is built on top of FlapwMBPTkutepov_linearized_2017 for the LQSGW part, and ComCTQMC for the quantum impurity problem solution [64]. We employed WIEN2K [49] to calculate the DFT band structures.

[64] C. Melnick, P. Sémon, K. Yu, N. D'Imperio, A.-M. Tremblay, and G. Kotliar, Accelerated impurity solver for DMFT and its diagrammatic extensions, Comput. Phys. Commun. **267**, 108075 (2021).

[65] Y.-F. Li, S.-D. Chen, M. Garcia-Diez, M. Iraola, H. Pfau, Y.-L. Zhu, Z.-Q. Mao, T. Chen, M. Yi, P.-C. Dai *et al.*, Spectroscopic evidence for topological band structure in $FeTe_{0.55}Se_{0.45}$, arXiv:2307.03861.

[66] From the even parity of the Fe(d_{xy}) wave function and the odd parity of the Se(p_z) wave function.

[67] The $4\tilde{t}_1$, $4\tilde{t}_2$, and $(\tilde{\epsilon}_{xy} - 4\tilde{t}_{xy})$-$(\tilde{\epsilon}_{p_z} + 4\tilde{t}_{p_z})$ terms for the LQS*GW* + DMFT results are 1.200, 0.892, and 2.642 eV, respectively (see SM [43], Sec. VII).

[68] We confirmed that the simulation of the $FeSe_{1-x}Te_x$ alloy from the effective FeSe lattice is possible, and one can simulate the Te ratio enhancement in the alloy from the Se height enhancement of the effective FeSe lattice. See Sec. IV of SM [43].
[69] See Fig. S21 of SM [43] for the correlation-induced renormalization of t_1 dominantly effects on the xy^- band.
[70] K.-D. Richler, S. Fratini, S. Ciuchi, and D. Mayou, Inhomogeneous dynamical mean-field theory of the small polaron problem, J. Phys. Condens. Matter **30**, 465902 (2018).
[71] M. Li, G. Li, L. Cao, X. Zhou, X. Wang, C. Jin, C.-K. Chiu, S. J. Pennycook, Z. Wang, and H.-J. Gao, Ordered and tunable Majorana-zero-mode lattice in naturally strained LiFeAs, Nature (London) **606**, 890 (2022).